

ORIGINAL ARTICLE

Structure analyses of polybutadiene rubber crosslinked with unsaturated carboxylate using contrast variation small-angle neutron scattering

Ryo Mashita¹, Hiroyuki Kishimoto¹, Rintaro Inoue² and Toshiji Kanaya³

We studied the structure of polybutadiene rubber (BR) crosslinked with zinc diacrylate (ZDA) to elucidate the structure of the high crosslink density BR using a contrast variation small-angle neutron scattering (CV-SANS) method. $S_{PP}(q)$, $S_{ZZ}(q)$ and $S_{PZ}(q)$, which correspond to the partial scattering functions of the self-correlation of BR, the self-correlation of ZDA aggregates and the cross-correlation between BR and ZDA aggregates, respectively, were successfully evaluated using CV-SANS. A model function assuming a hierarchical structure consisting of spheres with broad size distributions was used to describe the $S_{ZZ}(q)$, and the careful analysis of $S_{PZ}(q)$ revealed the existence of a HC-BR layer around the ZDA aggregates owing to an inhomogeneous crosslinked structure in the BR matrix. This is the first time quantitative structural analysis of the HC-BR layer in this rubber material has been performed. In addition, the network structure of the HC-BR layer in the rubber matrix is responsible for the high mechanical modulus of the rubber.

Polymer Journal (2016) 48, 239–245; doi:10.1038/pj.2015.102; published online 28 October 2015

INTRODUCTION

Rubber materials, which are utilized in various industrial products, such as tires for automobiles, airplanes and base-isolating devices, are indispensable in industry and our daily life.

Rubber that is crosslinked with metal diacrylate exhibits strong reinforcement properties without the addition of reinforcing materials, such as carbon black, silica and clay, and therefore, the structure of this rubber has been extensively studied. The aggregates of metal ions with sizes of 1–30 nm^{1–5} were previously assumed to be responsible for the mechanical properties of these materials, and many researchers have focused on structural analyses of the metal ion aggregates in these rubber materials^{6–10} to improve the mechanical properties of these material. In contrast to expectations, no dramatic improvement in the mechanical properties has been reported despite extensive studies. In contrast, the structure of the rubber matrix, which occupies a majority of the volume fraction in rubber materials, has not been studied owing to its structural complexity. The elucidation of the structure of the rubber matrix could offer a promising approach for enhancing the mechanical properties of these rubber materials, and therefore, we decided to study the structure of the rubber matrix in itself. Preliminary transverse proton (¹H) nuclear magnetic resonance relaxation measurements have revealed the existence of two relaxation

processes in the rubber matrix,¹¹ implying the coexistence of high and low crosslink density regions in the rubber matrix. To confirm the existence of these two regions possessing different crosslink densities, transmission electron microscopic (TEM) and scanning electron microscopic measurements have been performed on the rubber matrix. However, the coexistence of these two regions in the rubber matrix has not been clarified owing to the lack of contrast in both measurements.

In our previous study,⁵ we investigated the coexistence of high and low crosslink density regions in a rubber matrix using a good solvent and the complementary use of small-angle X-ray scattering (SAXS) and small-angle neutron scattering (SANS) by assuming that the degree of swelling for each region would be different. The coexistence of high and low crosslink density BR (HC-BR) regions in the rubber matrix was successfully determined. Based on SAXS and SANS results, the HC-BR region may be absorbed on the surface of metal ion aggregates. However, we have not experimentally confirmed this hypothesis. Therefore, another experimental approach is essential for understanding both the structure and physical properties of HC-BR in more detail.

The contrast variation SANS (CV-SANS) method is a powerful tool for structural analyses of multicomponent systems, such as

¹Material Research and Development Hqs., SUMITOMO Rubber Industries, LTD., Kobe, Japan; ²Research Reactor Institute, Kyoto University, Osaka, Japan and ³Institute for Chemical Research, Kyoto University, Kyoto-fu, Japan

Correspondence: R Mashita, Material Research and Development Hqs., SUMITOMO Rubber Industries, LTD, 1-1,2-Chome, Tsutsui-cho, Chuo-ku, Kobe, Hyogo 651-0071, Japan.

E-mail: r-mashita.az@srigroup.co.jp

or Associate professor R Inoue, Research Reactor Institute, Kyoto University, 2, Asashironishi, Kumatori-cho, Sennan-gun, Osaka 590-0494, Japan.

E-mail: rintaro@rri.kyoto-u.ac.jp

or Professor T Kanaya, Institute for Chemical Research, Kyoto University, Uji, Kyoto-fu 611-0011, Japan.

E-mail: kanaya@scl.kyoto-u.ac.jp

Received 2 July 2015; revised 31 August 2015; accepted 1 September 2015; published online 28 October 2015

clay–polymer and silica–polymer systems,^{12–16} and the advantage of this method is the evaluation of the partial scattering functions through modulation of scattering length densities of the solvents. Using this method, Endo *et al.*¹⁶ determined whether or not a polymer was adsorbed on the surface of nanocomposites based on the sign of the partial scattering function of the cross-correlation term, which describes the intercorrelation between the components. Therefore, we performed a more detailed structural analysis of HC-BR using the CV-SANS method.

In this study, the structural relationship between the metal ion aggregates and the HC-BR region as well as the hierarchical structure of metal aggregates and the network structures in matrix BR were investigated using CV-SANS.

EXPERIMENTAL PROCEDURE

Materials and sample preparation

The details of the materials used in this study are summarized in Table 1. We used polybutadiene (BR; BR730, JSR Co., Ltd., Tokyo, Japan.) with weight-average molecular weight (M_w) of 6.72×10^5 and molecular weight distribution index (M_w/M_n) of 2.39, where M_n is number-average molecular weight as the rubber matrix. The content of *cis*, *trans* and *vinyl* in the BR was 97, 2 and 1%, respectively. Zinc diacrylate (ZDA; Sanceler SR, Sanshin Chemical Industry Co., Ltd., Yanai, Yamaguchi, Japan.) and dicumyl peroxide (DCP; Percmyl D, Nichiyu Co., Ltd., Tokyo, Japan.) were used as a crosslinker and an initiator, respectively, in the crosslinking reaction. BR, ZDA and DCP with a volume ratio of 87.3, 12.4 and 0.3, respectively, were placed into a 6-inch two-roll mill simultaneously and mixed for 5 min at room temperature. After mixing at room temperature, the mixture consisting of BR, ZDA and DCP was placed into a mold and heated at 170 °C for 20 min to promote the chemical reaction. Prior to the SANS and SAXS measurements, the samples were swollen in a mixed solvents containing hydrogenated toluene (*h*-toluene) and deuterated toluene (*d*-toluene) until their equilibrium states were reached at room temperature (final swollen ratio was ~196%). The swollen samples were measured in a quartz cell that was 2 mm thick. For the TEM observation, the sample, which had a thickness of 50 nm, was prepared using a microtome.

Measurements

The SANS measurements were performed with a 40 m SANS spectrometer installed at a neutron scattering facility (HANARO) in Daejeon, Korea. The wavelength (λ) of the incident neutron and its distribution ($\Delta\lambda/\lambda$) were 7.49 Å and 0.12, respectively. In addition to the three different sample-to-detector distances of 1.16, 4.7 and 19.95 m, a focusing lens was also utilized to access a lower q region than that covered by the normal set-up. Using this set-up, the q values ranged from 2.0×10^{-2} to $7.5 \times 10^{-1} \text{ nm}^{-1}$. The observed two-dimensional scattering images were circularly averaged to obtain one-dimensional scattering curves, which were corrected for the backgrounds from the sample cell and air, electronic noise, detector sensitivity and transmittance of the neutrons through the samples and incoherent scattering. The SANS scattering intensity was converted to an absolute intensity scale (cm^{-1}) using the direct beam flux method.

SAXS measurements were also conducted on the same samples. The SAXS measurements were performed using a BL03XU instrument installed at a synchrotron radiation X-ray scattering facility (SPring-8) in Nishiharima, Japan, and the incident wavelength of the X-ray and the sample-to-detector distance were 1.5 Å and 3.0 m, respectively. Ultra small-angle X-ray scattering (USAXS) measurements were also performed with a BL20XU instrument installed at SPring-8, and the incident wavelength of the X-ray and the sample-to-detector

Table 1 Characteristics of the components of the samples used in the current study

Polybutadiene (vol%)	87.3
Zinc diacrylate (vol%)	12.4
Dicumyl peroxide (vol%)	0.3

distance were 0.54 Å and 160.5 m, respectively. By combining the SAXS and USAXS measurements, we can cover a q range from 2.9×10^{-3} to $8.7 \times 10^{-1} \text{ nm}^{-1}$. The two-dimensional scattering images were circularly averaged to obtain one-dimensional scattering curves, which were corrected for the backgrounds from the sample cell and the air as well as for the transmittance of the X-rays through the samples.

TEM measurements were performed at operating voltages of 200 kV under dark-field mode.

Dynamic viscoelasticity measurements were carried out with a dynamic mechanical analyzer (RSA-G2, TA Instruments Japan Inc., Tokyo, Japan) at 303 K and 10 Hz.

Differential scanning calorimetric measurements were carried out with a differential scanning calorimeter (Q200, TA Instruments Japan Inc.) for a temperature range of -150 to 150 °C at a rate of 10 °C min^{-1} .

RESULTS AND DISCUSSION

Roughly, two types of ZDA aggregates with diameters of ~5 nm (first ZDA aggregates) and ~20 nm (second ZDA aggregates) were observed in the TEM image, as shown in Figure 1. Because this TEM image was taken in the dark-field mode, the bright particles correspond to ZDA aggregates where the rubber material has a high electron density. Although it is difficult to accurately analyze the TEM image owing to its limited spatial resolution, a wide distribution of sizes and a hierarchical structure over a wide range of spatial scales was observed for ZDA aggregates in the BR matrix. In addition, micrometer-sized ZDA aggregates were also observed in our previous study⁵ in the BR/ZDA system, suggesting the coexistence of nanometer- and micrometer-sized ZDA aggregates in the same sample after the chemical reaction.

Figure 2 shows the SANS profiles $I(q)$ of BR crosslinked with ZDA and swollen by toluene consisting of a different mixing ratio of *h*-toluene and *d*-toluene. The Kratky plots ($q^2I(q)$ vs q) are shown in the inset to visualize the change in the q dependence of $I(q)$. The scattering intensity ($I(q)$) tends to decrease as the ratio of *d*-toluene in toluene solvent decreased, reflecting the decrease in the scattering contrast between BR and the toluene solvent. However, the q dependence of $I(q)$ is strongly dependent on the ratio of *d*-toluene in the toluene solvent. In particular, the q dependence of $I(q)$ swollen by 100% *d*-toluene differs from that swollen by 100% *h*-toluene. If the rubber

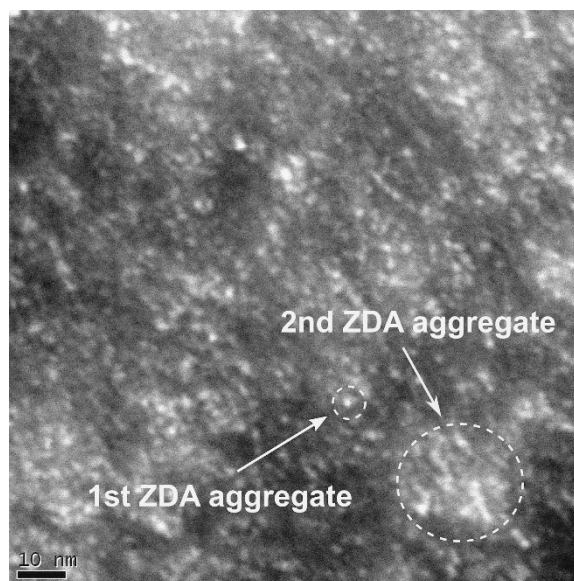


Figure 1 TEM image. A full color version of this figure is available at the *Polymer Journal* online.

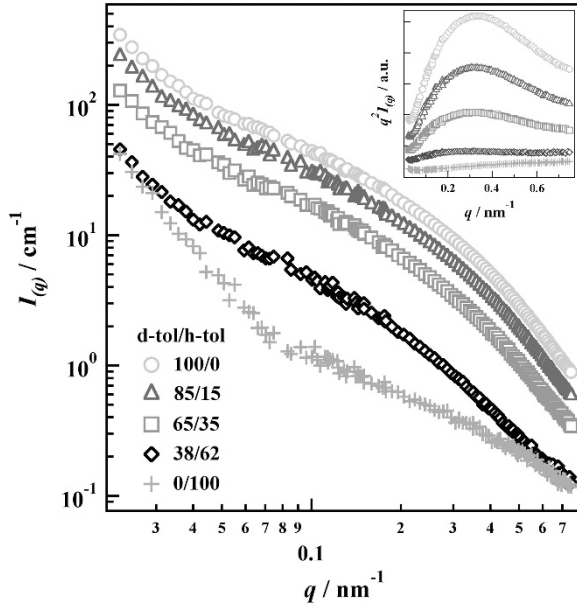


Figure 2 SANS profiles for the material swollen in a mixture of *d*-toluene and *h*-toluene. The inset shows the Kratky plots of each solvent. A full color version of this figure is available at the *Polymer Journal* online.

Table 2 Scattering length densities and electron densities of the materials used in the current study

	Scattering length density ($\times 10^{-6} \text{ \AA}^{-2}$)	Electron density ($\times 10^{23} \text{ electron cm}^{-3}$)
Polybutadiene	0.42	3.01
Zinc diacrylate	2.15	4.83
Toluene	0.94	2.83
Deuterated toluene	5.66	2.82

matrix swells homogeneously in the toluene solvent, the q dependence of $I(q)$ must be independent of the fraction of *d*-toluene in the toluene solvent. These experimental results imply that a component other than the ZDA aggregates and BR matrix must exist in the current rubber material.

In principle, our samples can be regarded as a four-component system consisting of BR, ZDA, DCP and toluene solvent. However, the volume fraction of DCP included in our sample is negligibly small compared with the other components, as shown in Table 1. Therefore, our sample can be approximately regarded as three components consisting of BR, ZDA and the toluene solvent. Under such an approximation, $I(q)$ can be expressed as follows:

$$I(q) = (\sigma_p - \sigma_{sol})^2 S_{pp}(q) + 2(\sigma_p - \sigma_{sol})(\sigma_z - \sigma_{sol}) S_{pz}(q) + (\sigma_z - \sigma_{sol})^2 S_{zz}(q) \quad (1)$$

where σ_p , σ_z and σ_{sol} are the scattering length densities of BR, ZDA and the solvent, respectively, as shown in Table 2. The scattering length density of the solvent is calculated by considering the mixing ratio of *h*-toluene and *d*-toluene. $S_{pp}(q)$, $S_{zz}(q)$ and $S_{pz}(q)$ are the partial scattering functions of the self-correlation of BR, the self-correlation of the ZDA aggregates and the cross-correlation between the BR and ZDA aggregates, respectively. If the SANS measurements are performed at n different toluene solvents consisting of different

mixing ratios of *h*-toluene and *d*-toluene, each $I_j(q)$ ($1 \leq j \leq n$) is related to the ($S_{pp}(q)$, $S_{zz}(q)$ and $S_{pz}(q)$) partial scattering functions as follows:

$$\begin{pmatrix} I_1(q) \\ I_2(q) \\ \vdots \\ I_n(q) \end{pmatrix} = \begin{pmatrix} {}^1\Delta\sigma_p^2 & {}^1\Delta\sigma_p^1\Delta\sigma_z & {}^1\Delta\sigma_z^2 \\ {}^2\Delta\sigma_p^2 & {}^2\Delta\sigma_p^2\Delta\sigma_z & {}^2\Delta\sigma_z^2 \\ \vdots & \vdots & \vdots \\ {}^n\Delta\sigma_p^2 & {}^n\Delta\sigma_p^n\Delta\sigma_z & {}^n\Delta\sigma_z^2 \end{pmatrix} \begin{pmatrix} S_{pp}(q) \\ S_{pz}(q) \\ S_{zz}(q) \end{pmatrix} \quad (2)$$

where

$$\Delta\sigma_p = \sigma_p - \sigma_{sol} \quad (3)$$

$$\Delta\sigma_z = \sigma_z - \sigma_{sol} \quad (4)$$

$S_{pp}(q)$, $S_{zz}(q)$ and $S_{pz}(q)$ can be calculated according to the singular value decomposition algorithm.¹⁶

$$\begin{pmatrix} S_{pp}(q) \\ S_{pz}(q) \\ S_{zz}(q) \end{pmatrix} = \begin{pmatrix} {}^1\Delta\sigma_p^2 & {}^1\Delta\sigma_p^1\Delta\sigma_z & {}^1\Delta\sigma_z^2 \\ {}^2\Delta\sigma_p^2 & {}^2\Delta\sigma_p^2\Delta\sigma_z & {}^2\Delta\sigma_z^2 \\ \vdots & \vdots & \vdots \\ {}^n\Delta\sigma_p^2 & {}^n\Delta\sigma_p^n\Delta\sigma_z & {}^n\Delta\sigma_z^2 \end{pmatrix}^{-1} \begin{pmatrix} I_1(q) \\ I_2(q) \\ \vdots \\ I_n(q) \end{pmatrix} \quad (5)$$

Figures 3a–c show the calculated partial scattering functions ($S_{zz}(q)$, $S_{pp}(q)$ and $S_{pz}(q)$, respectively). $I(q)$ from the SAXS measurement ($I_{SAXS}(q)$) is also shown in Figure 3a. Because the difference in the electron density between ZDA and toluene is much larger than those of the other components in the SAXS experiment, as shown in Table 2, the scattering intensity from ZDA dominates the total scattering intensity for the SAXS measurements. Under such an assumption, the q dependence of $I_{SAXS}(q)$ is expected to reproduce the q dependence of $S_{zz}(q)$. As shown in Figure 3a, the q dependence of $I_{SAXS}(q)$ was consistent with that of $S_{zz}(q)$, supporting the validity of the evaluation of the partial scattering function. To quantitatively characterize the obtained $S_{pp}(q)$, $S_{zz}(q)$ and $S_{pz}(q)$, an appropriate model should be assumed. The model proposed by Takenaka *et al.*,¹³ who studied rubber–silica systems with the SANS techniques, was employed to model the current rubber material consisting of ZDA aggregates, a HC-BR layer surrounding the ZDA aggregates with a volume fraction of BR in the swollen HC-BR layer with toluene (ϕ_{HC-BR}) and the BR matrix with a volume fraction of BR in the swollen matrix BR region with toluene (ϕ_{MT-BR}) (Figure 4). Based on this model, the partial scattering functions can be described as follows¹³:

$$S_{zz}(q) = F_{ZDA}^2(q) \quad (6)$$

$$S_{pz}(q) = (\phi_{HC-BR} - \phi_{MT-BR}) F_{HC-BR+ZDA}(q) F_{ZDA}(q) - \phi_{HC-BR} F_{ZDA}^2(q) \quad (7)$$

$$S_{pp}(q) = [(\phi_{HC-BR} - \phi_{MT-BR}) F_{HC-BR+ZDA}(q) - \phi_{HC-BR} F_{ZDA}(q)]^2 + S_{pp,nt}(q) + S_{pp,ih1}(q) + S_{pp,ih2}(q) \quad (8)$$

where

$$S_{pp,nt}(q) = \frac{S_{pp,nt}^0(0)}{1 + q^2 \xi_1^2} \quad (9)$$

$$S_{pp,ih1}(q) = \frac{S_{pp,ih1}^0(0)}{(1 + q^2 \xi_2^2)^2} \quad (10)$$

$$S_{pp,ih2}(q) = \frac{S_{pp,ih2}^0(0)}{(1 + q^2 \xi_3^2)^2} \quad (11)$$

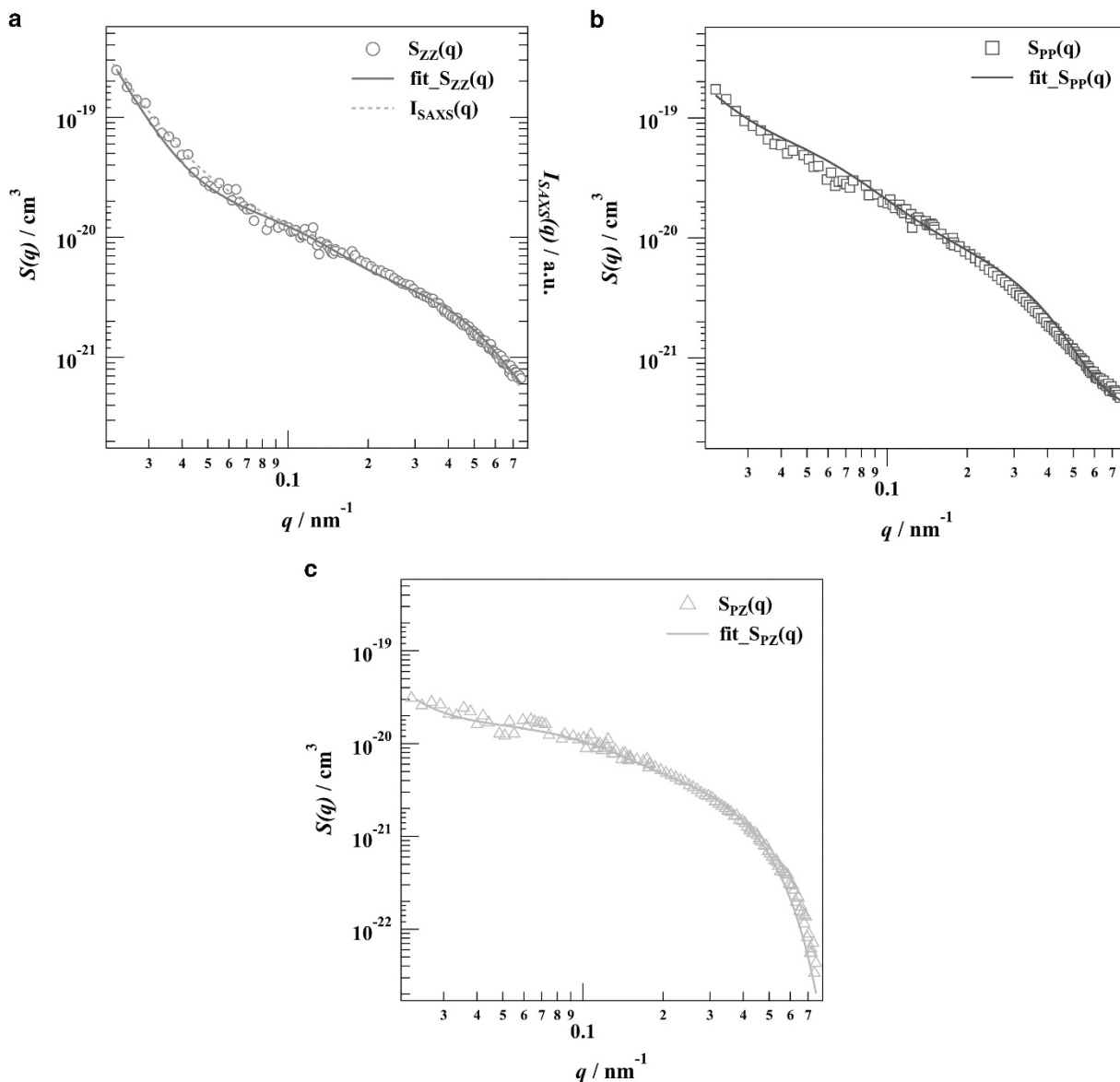


Figure 3 Partial scattering functions (a) $S_{ZZ}(q)$, (b) $S_{PP}(q)$ and (c) $S_{PZ}(q)$ obtained using the CV-SANS method. Dashed line in **a** is the SAXS profile. Solid lines represent the results from the fitting with the model function. A full color version of this figure is available at the *Polymer Journal* online.

$F_{ZDA}(q)$ and $F_{HC-BR+ZDA}(q)$ are the scattering amplitudes of the ZDA aggregates and the region consisting of ZDA aggregates and the HC-BR layer, respectively. Three correlation lengths due to the crosslinking network, inhomogeneous crosslinking and larger inhomogeneous crosslinking have been reported for similar rubber materials.^{14,15} Therefore, three scattering functions ($S_{pp,nt}(q)$, $S_{pp,ih1}(q)$ and $S_{pp,ih2}(q)$) are introduced to describe the concentration fluctuation of the BR network structure ($S_{pp,nt}(q)$), inhomogeneous crosslinked structure ($S_{pp,ih1}(q)$) and larger inhomogeneous crosslinked structure ($S_{pp,ih2}(q)$) in the BR matrix region in Equation (9). ξ_1 , ξ_2 , ξ_3 , $S_{pp,nt}^0(0)$, $S_{pp,ih1}^0(0)$ and $S_{pp,ih2}^0(0)$ are the correlation lengths of the BR network, the inhomogeneous crosslinked structure and the larger inhomogeneous crosslinked structure in BR matrix region as well as the prefactors of the inhomogeneous crosslinked structure and the larger inhomogeneous crosslinked structure in matrix BR region, respectively. Assuming the absence of an adsorbed BR layer on the surface of the ZDA aggregates, Equation (7) can be approximated as

follows¹⁶:

$$S_{pz}(q) = -\phi_{MT-BR} F_{ZDA}^2(q) \quad (12)$$

In the current experiment, the $S_{pz}(q)$ has a positive sign in the q range examined, implying the possibility of the existence of cross-correlation between BR and ZDA based on structural analysis. Other experimental proof for the existence of an adsorbed BR layer on the surface of the ZDA aggregates was obtained from the differential scanning calorimetric results (Figure 5). The endothermic peak observed at approximately 0 °C originated from the crystal melting peak owing to the high *cis* content in the BR matrix. After the chemical reaction with ZDA, new endothermic behavior, which was not detected for the BR matrix (non-crosslinked BR), was observed at approximately 90 °C. It is important to note that the endothermic behavior at 90 °C was not observed for either the ZDA monomer or self-polymerized ZDA.¹⁷ Therefore, the endothermic behavior observed at 90 °C must originate from BR crosslinked with ZDA. The interfacial polymer layer near the

impenetrable substrate or nanoparticle exhibits anomalous physical properties, and one representative example is the dramatic increase in the glass transition temperature (T_g).^{18,19} Then the endothermic behavior at 90 °C in the rubber material must correspond to the second T_g from the HC-BR layer originating from the crosslinking reaction between BR and ZDA. Based on structural analysis and thermal properties, the existence of a HC-BR layer can be confirmed.

Based on our previous TEM and scanning electron microscopic studies on BR crosslinked with ZDA,⁵ both the hierarchical structure of the ZDA aggregate and the broad size distributions of the ZDA aggregates have been observed. In addition, the morphologies of the ZDA aggregates were approximately sphere shaped. Therefore, the $S_{ZZ}(q)$ partial scattering function can be expressed by the model function considering the hierarchical structure of the form factor of spheres with broad size distributions.

$$S_{ZZ}(q) = |F_{ZDA}(q)|^2 = n_{ZDA3} \int_0^\infty P(r, r_{0,ZDA3}, \sigma_{ZDA3}) \left(\frac{4}{3}\pi r^3\right)^2 \left(\frac{3|\sin(qr) - qr \cos(qr)|}{(qr)^3}\right)^2 dr + n_{ZDA2} \int_0^\infty P(r, r_{0,ZDA2}, \sigma_{ZDA2}) \left(\frac{4}{3}\pi r^3\right)^2 \left(\frac{3|\sin(qr) - qr \cos(qr)|}{(qr)^3}\right)^2 dr + n_{ZDA1} \int_0^\infty P(r, r_{0,ZDA1}, \sigma_{ZDA1}) \left(\frac{4}{3}\pi r^3\right)^2 \left(\frac{3|\sin(qr) - qr \cos(qr)|}{(qr)^3}\right)^2 dr \quad (13)$$

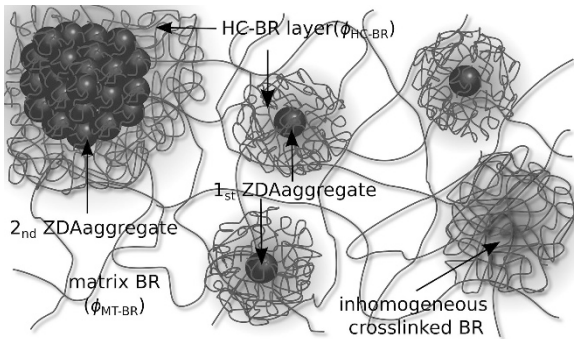


Figure 4 Schematic representation of the ZDA/BR system swollen by the solvent. A full color version of this figure is available at the *Polymer Journal* online.

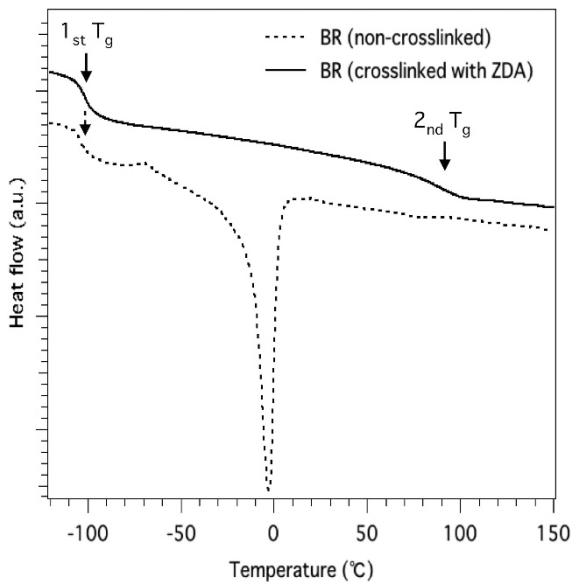


Figure 5 DSC curves of non-crosslinked and crosslinked BR.

where

$$P(r, r_{0,i}, \sigma_i) = \frac{1}{\sqrt{2\pi\sigma_i^2}} \exp\left(-\frac{(r - r_{0,i})^2}{2\sigma_i^2}\right) \quad (14)$$

$$i = ZDA1, ZDA2, ZDA3 \quad (15)$$

$r_{0,ZDA1}$, $r_{0,ZDA2}$ and $r_{0,ZDA3}$ are the mean radii of the first ZDA aggregates, the second ZDA aggregates and the larger ZDA aggregates, respectively. It is important to note that we used a value of 1.6 μm for $r_{0,ZDA3}$, which was determined in our previous study⁵ because the size of $r_{0,ZDA3}$ is beyond the accessible q range in the current SANS measurements. n_{ZDA1} , n_{ZDA2} and n_{ZDA3} are the number per unit volume of the first ZDA aggregates, second ZDA aggregates and the larger ZDA aggregates, respectively. To describe the size distribution of the ZDA aggregates, a Gaussian distribution was used, as described in Equation (13). The solid line was able to reproduce the observed $S_{ZZ}(q)$, as shown in Figure 3a, and then we adapted this model function.

Because the HC-BR layer is supposed to adsorb onto the surface of ZDA aggregates, the scattering function of the region consisting of ZDA aggregates and the HC-BR layer ($S_{HC-BR+ZDA}(q)$) is also expected to be described with a similar hierarchical structure model as follows:

$$S_{HC-BR+ZDA}(q) = |F_{HC-BR+ZDA}(q)|^2 = n_{ZDA3} \int_0^\infty P(r, r_{0,HC-BR3}, \sigma_{HC-BR3}) \left(\frac{4}{3}\pi r^3\right)^2 \left(\frac{3|\sin(qr) - qr \cos(qr)|}{(qr)^3}\right)^2 dr + n_{ZDA2} \int_0^\infty P(r, r_{0,HC-BR2}, \sigma_{HC-BR2}) \left(\frac{4}{3}\pi r^3\right)^2 \left(\frac{3|\sin(qr) - qr \cos(qr)|}{(qr)^3}\right)^2 dr + n_{ZDA1} \int_0^\infty P(r, r_{0,HC-BR1}, \sigma_{HC-BR1}) \left(\frac{4}{3}\pi r^3\right)^2 \left(\frac{3|\sin(qr) - qr \cos(qr)|}{(qr)^3}\right)^2 dr \quad (16)$$

where $r_{0,HC-BR1}$, $r_{0,HC-BR2}$ and $r_{0,HC-BR3}$ are the mean radii of the first HC-BR layer, the second HC-BR layer and the larger HC-BR layer, respectively. Figure 3 shows the results for the fitting analyses of the partial scattering functions. Each partial scattering function fitted well to the previously mentioned structure models, and the parameters obtained from the fitting procedures are summarized in Table 3. From the calculated partial scattering function $S_{ZZ}(q)$ corresponding to self-correlation of the ZDA aggregates, the size of the ZDA aggregates can be evaluated. The mean size of the first and second ZDA aggregates coincided with those determined from image analyses on the TEM images within experimental error ($r_{0,ZDA1} = 1.4$ nm and $r_{0,ZDA2} = 5.0$ nm). This result indicates that the difference in the measurement condition between SANS and TEM does not affect the resulting size information for the ZDA aggregates, which are on the nanometer scale. ϕ_{HC-BR} and ϕ_{MT-BR} are 0.89 and 0.46, respectively, implying that the swelling ratio of HC-BR was lower than that of the BR matrix. Therefore, the crosslinking density of the HC-BR layer around the ZDA aggregates must be higher than that of the BR matrix region. The physical description of HC-BR, which segregated on the

Table 3 Characteristic parameters calculated from the fitting analysis

$r_{0,ZDA1}$ (nm)	1.4	$r_{0,HC-BR1}$ (nm)	3.2
$r_{0,ZDA2}$ (nm)	5.0	$r_{0,HC-BR2}$ (nm)	7.9
$r_{0,ZDA3}$ (nm)	1600	$r_{0,HC-BR3}$ (nm)	1610
σ_{ZDA1} (nm)	1.1	σ_{HC-BR1} (nm)	0.3
σ_{ZDA2} (nm)	1.7	σ_{HC-BR2} (nm)	1.8
σ_{ZDA3} (nm)	800	σ_{HC-BR3} (nm)	800
n_{ZDA1} (nm ⁻³)	3.8×10^{-3}	ϕ_{HC-BR}	0.89
n_{ZDA2} (nm ⁻³)	1.1×10^{-6}	ϕ_{MT-BR}	0.46
n_{ZDA3} (nm ⁻³)	6.5×10^{-18}	ξ_1 (nm)	2.6
ξ_2 (nm)	8.2	ξ_3 (nm)	61

surface of the ZDA aggregates, was experimentally confirmed, and successful investigation of the structure of the HC-BR layer was achieved.

The volume fraction of the BR matrix region (ϕ_{MT-BR}) was compared with that from the degree of swelling of the sample Q (1.96). Because ZDA cannot be swollen but BR can be swollen in toluene, ϕ_{MT-BR} estimated from Q can be expressed as follows:

$$\phi_{MT-BR} = \frac{\Psi_{BR}}{\Psi_{BR} + Q - 1} = \frac{0.873}{0.873 + 1.96 - 1} = 0.48 \quad (17)$$

where Ψ_{BR} is the volume fraction of BR. The value of ϕ_{MT-BR} evaluated from Q is nearly equal to that obtained from the SANS measurement (that is, 0.46), suggesting that the results from the fitting analyses are reasonable.

Based on the $r_{0,ZDA1}$ (1.4 nm) and $r_{0,HC-BR1}$ (3.2 nm) values, the mean thicknesses of the HC-BR layer around the first ZDA aggregates was estimated to be 1.8 nm, and the thickness of the HC-BR layer around the second ZDA aggregates was estimated to be 2.9 nm using the same assumption. The total volume fraction of ZDA aggregates ($\phi_{total-ZDA,fit}$) and HC-BR layers ($\phi_{total-HC-BR,fit}$) were estimated to 0.062 and 0.075, respectively. In comparison to the initial volume fraction of ZDA (0.124), $\phi_{total-ZDA,fit}$ was approximately half that value. Therefore, the model function is not suitable for the current rubber material. However, it is important to note that the rubber material was swollen by toluene for the SANS and SAXS experiments. Therefore, we must take into account the contribution of toluene for comparison to the volume fraction of ZDA. For this purpose, $\phi_{total-ZDA,fit}$ and $\phi_{total-HC-BR,fit}$ should be normalized by the degree of swelling (Q), and these normalized values ($\phi_{total-ZDA,fit}$ and $\phi_{total-HC-BR,fit}$) were determined to be 0.122 and 0.147, respectively. Taking account the possible error from the fitting procedure, $\phi_{total-ZDA,fit}$ is nearly equal to the ZDA content of the sample (0.124), suggesting that the results from the fitting analyses are reasonable.

The ξ_1 , ξ_2 and ξ_3 values, which indicate that the distance between the crosslinking and the size of the inhomogeneous crosslinked structures in the BR matrix region, are 2.6, 8.2 and 61 nm, respectively. We also estimated the average molecular weight between the crosslinks (M_S) from the degree of swelling of the sample ($Q=1.96$) using the Flory–Rehner equation.^{20,21} Then M_S was estimated to be $4.22 \times 10^2 \text{ g mol}^{-1}$. The correlation length (ξ_s) of the BR network can be calculated from the following equation:

$$M_S = M_0 \left(\frac{\xi_s}{l} \right)^{1.67} \quad (18)$$

where M_0 and l are the molecular weight of the monomer of BR and the statistical segment length of BR, respectively. Using $M_0 = 52 \text{ g mol}^{-1}$ and $l = 0.828 \text{ nm}$, ξ_s was calculated to be 3.1 nm. The ξ_s value (3.1 nm) that was obtained from the degree of swelling nearly coincided with the ξ_1 value (2.6 nm) from CV-SANS analysis, suggesting that the adopted analysis model in the current study is reasonable.

In comparison to rubber material reinforced by the addition of an inorganic nanofiller, such as carbon black, which is phase separated in the rubber matrix, a substantial reinforcement effect was observed for the current rubber, as described in Introduction section (Figure 6). Therefore, the additional contribution beyond the addition of a small-sized filler must be a key factor for realizing high mechanical strength in the current material. Next, we discuss the origin of the substantial increase in the mechanical strength of the current system from the viewpoint of structural analysis. The mean distance between the first

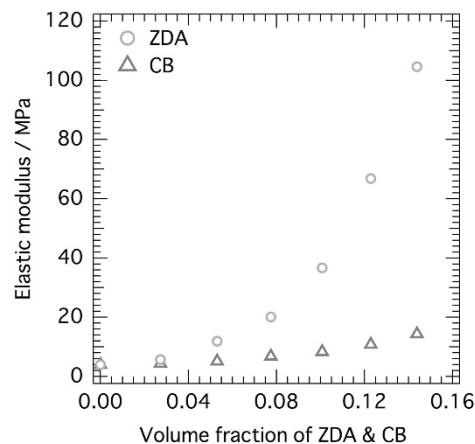


Figure 6 Relationship between the elastic modulus and the volume fraction of ZDA and CB. A full color version of this figure is available at the *Polymer Journal* online.

ZDA aggregates is roughly estimated to be 1–5 nm in the TEM image (Figure 1). Based on the radius of the ZDA aggregates and the thickness of the HC-BR layer obtained from CV-SANS, the HC-BR layer may serve to connect the ZDA aggregates to each other. Alternatively, the nanometer-sized ZDA aggregates may have a major role as a cross-linker in the current system. In addition, the sum of the volume fraction of the ZDA aggregates ($\phi_{total-ZDA,fit}$) and the HC-BR layers ($\phi_{total-HC-BR,fit}$) is only 0.269, which is lower than the fraction of closest packing. A network of HC-BR layers may be responsible for the high mechanical strength of the current rubber material. In addition, the micrometer-sized aggregates may act as stiff fillers in the current system even though the detailed structural analysis is challenging owing to limitations in the accessible q range.

In current study,⁵ accurate information was simultaneously extracted for both the structure of the HC-BR layer around ZDA aggregates. Because the thickness and volume fraction of the HC-BR layer were quantitatively revealed for the first time, additional improvement in the mechanical properties of the rubber materials must be accomplished by controlling the structure of the HC-BR region.

SUMMARY

We investigated the structure of butadiene rubber (BR) crosslinked with ZDA using the CV-SANS method with a focus on the structure of the high crosslink density BR (HC-BR) layer surrounding the ZDA aggregates. The partial scattering functions ($S_{pp}(q)$, $S_{zz}(q)$ and $S_{pz}(q)$) were obtained using the CV-SANS method and singular value decomposition. The q dependence of $I_{SAXS}(q)$ was quite similar to that of $S_{zz}(q)$, suggesting that the results of the CV-SANS method and singular value decomposition are reasonable. $S_{zz}(q)$ fitted well to the model assuming a hierarchical structure of spheres with broad size distributions. The analyses of $S_{pp}(q)$ and $S_{pz}(q)$ revealed the existence of a HC-BR layer surrounding the ZDA aggregates and an inhomogeneous crosslinked structure in the BR matrix region. The total volume fractions of ZDA aggregates ($\phi_{total-ZDA,fit}$) and the HC-BR layers ($\phi_{total-HC-BR,fit}$) were estimated to be 0.122 and 0.147, respectively, using the CV-SANS method. The sum of $\phi_{total-ZDA,fit}$ and $\phi_{total-HC-BR,fit}$ is only 0.269, which is lower than the fraction of closest packing, suggesting that HC-BR consists of a network, and this network structure in BR may be responsible for the high mechanical strength of the current rubber material. Using CV-SANS, our physical

description of HC-BR, which segregated on the surface of the ZDA aggregates, was experimentally confirmed. Therefore, the structure of the HC-BR layer was successfully achieved for the first time.

CONFLICT OF INTEREST

The authors declare no conflict of interest.

ACKNOWLEDGEMENTS

We thank Dr Young-Soo Han and Dr Tae-Hwan Kim of the Korea Atomic Energy Research Institute for their kind support in the SANS measurements at HANARO 40m SANS, Dr Hiroyasu Masunaga of the Japan Synchrotron Radiation Research Institute for his kind support in the SAXS measurements at SPring-8 BL03XU (Proposal Nos. 2011B 7260 and 2012A 7210) and Dr Yoshio Suzuki and Dr Akihisa Takeuchi of the Japan Synchrotron Radiation Research Institute and Dr Yuya Shinohara of Tokyo University for their kind support in the USAXS measurements at SPring-8 BL20XU (Proposal Nos. 2011B 1244 and 2012A 1686).

- Nagata, N., Sato, T., Fujii, T. & Saito, Y. Structure and mechanical properties of hydrogenated NBR/Zinc di-methacrylate vulcanizates. *J. Appl. Polym. Sci.* **53**, 103–120 (1994).
- Yuan, X., Zhang, Y., Peng, Z. & Zhang, Y. In situ preparation of magnesium methacrylate to reinforce NBR. *J. Appl. Polym. Sci.* **84**, 1403–1408 (2002).
- Wei, Z., Lu, Y., Yan, S., Meng, Y. & Zhang, L. Dramatic influence of curing temperature on micro-nano structure transform of HNBR filled with zinc dimethacrylate. *J. Appl. Polym. Sci.* **124**, 288–295 (2012).
- Wei, Z., Lu, Y., Meng, Y. & Zhang, L. Improved understanding of in-situ polymerization of zinc dimethacrylate: the solid bulk polymerization. *Polymer* **53**, 1409–1417 (2012).
- Mashita, R., Kishimoto, H., Inoue, R. & Kanaya, T. Small-angle X-ray and neutron scattering analyses of highly crosslinked rubber with unsaturated carboxylic acid. *Polym. J.* **45**, 57–63 (2013).
- Chu, B. J., Wu, D. Q., Lundberg, R. D. & Macknight, W. J. Small-angle X-ray scattering (SAXS) studies of sulfonated polystyrene ionomers. 1. Anomalous SAXS. *Macromolecules* **26**, 994–999 (1993).
- Tsujita, Y., Yasuda, M., Takei, M., Kinoshita, T., Takizawa, A. & Yoshimizu, H. Structure of ionic aggregates of ionomers. 1. Variation in the structure of ionic aggregates with different acid content and degree of neutralization of ethylene and styrene ionomers. *Macromolecules* **34**, 2220–2224 (2001).
- Al-Hussein, M., Lohmeijer, B. G. G., Schubert, U. S. & de Jeu, W. H. Melt morphology of polystyrene-poly(ethylene oxide) metallo-supramolecular diblock copolymer. *Macromolecules* **36**, 9281–9284 (2003).
- Zhou, C. N., Chan, D. C. & Winey, I. K. Reconciling STEM and X-ray scattering data to determine the nanoscale ionic aggregate morphology in sulfonated polystyrene ionomers. *Macromolecules* **41**, 6134–6140 (2008).
- Seitz, E. M., Chan, D. C., Opper, L. K., Baughman, W. T., Wagener, B. K. & Winey, I. K. Nanoscale morphology in precisely sequenced poly(ethylene-co-acrylic acid) zinc ionomers. *J. Am. Chem. Soc.* **132**, 8165–8174 (2010).
- Shiga, K., Murakami, R., Shigemitsu, T., Kimura, H. & Kitago, T. Golf ball material and golf ball patent appl. No. 207716(JP) (2011).
- Miyazaki, S., Endo, H., Karino, T., Haraguchi, K. & Shibayama, M. Gelation mechanism of poly(*N*-isopropylacrylamide)-clay nanocomposite gels. *Macromolecules* **40**, 4287–4295 (2007).
- Takenaka, M., Nishitujii, S., Amino, N., Ishikawa, Y., Yamaguchi, D. & Koizumi, S. Structure analyses of swollen rubber-filler systems by using contrast variation SANS. *Macromolecules* **42**, 308–311 (2009).
- Ikeda, Y., Higashitani, N., Hijikata, K., Kukubo, Y., Morita, Y., Shibayama, M., Osaka, N., Suzuki, T., Endo, H. & Kohjiya, S. Vulcanization: new focus on a traditional technology by small-angle neutron scattering. *Macromolecules* **42**, 2741–2748 (2009).
- Suzuki, T., Osaka, N., Endo, H., Shibayama, M., Ikeda, Y., Asai, H., Higashitani, N., Kokubo, Y. & Kohjiya, S. Nonuniformity in cross-linked natural rubber as revealed by contrast-variation small-angle neutron scattering. *Macromolecules* **43**, 1556–1563 (2010).
- Endo, H., Schwahn, D. & Cölfen, H. On the role of block copolymer additives for calcium carbonate crystallization: Small angle neutron scattering investigation by applying contrast variation. *J. Chem. Phys.* **120**, 9410–9423 (2004).
- Tsuchida, J., Saito, Y., Sato, S., Yuki, U., Inayama, S., Tatewaki, Y., Okada, S., Shindo, A., Mikura, C., Fushihara, K. & Yamada, M. Thermal solid-state polymerization of a divalent metal salt of an unsaturated carboxylic acid and the effects of additives. *Polym. J.* **45**, 1007–1012 (2013).
- Jones, R. L. & Richards, R. W. *Polymers at Surface and Interfaces* (Cambridge University Press, Cambridge, UK, 1999).
- Inoue, R., Nakamura, M., Matsui, K., Kanaya, T., Nishida, K. & Hino, M. Distribution of glass transition temperature in multilayered poly(methyl methacrylate) thin film supported on a Si substrate as studied by neutron reflectivity. *Phys. Rev. E* **88**, 032601 (2013).
- Flory, P. J. & Rehner, J. Statistical mechanics of cross-linked polymer networks II. Swelling. *J. Chem. Phys.* **11**, 521 (1943).
- Kraus, G. Swelling of filler-reinforced vulcanizates. *J. Appl. Polym. Sci.* **7**, 861–871 (1963).